



# Multi-dimensional experimental and computational exploration of metabolism pinpoints complex probiotic interactions

Guido Zampieri<sup>a,b</sup>, Georgios Efthimiou<sup>c</sup>, Claudio Angione<sup>a,d,e,\*</sup>

<sup>a</sup> School of Computing, Engineering and Digital Technologies, Teesside University, Middlesbrough, United Kingdom

<sup>b</sup> Department of Biology, University of Padova, Padova, Italy

<sup>c</sup> Centre for Biomedicine, Hull York Medical School, Hull, United Kingdom

<sup>d</sup> Centre for Digital Innovation, Teesside University, Middlesbrough, United Kingdom

<sup>e</sup> National Horizons Centre, Teesside University, Darlington, United Kingdom

## ARTICLE INFO

### Keywords:

Probiotics  
Metabolic modelling  
Biofilms  
Microbial interactions  
Multivariate analysis

## ABSTRACT

Multi-strain probiotics are widely regarded as effective products for improving gut microbiota stability and host health, providing advantages over single-strain probiotics. However, in general, it is unclear to what extent different strains would cooperate or compete for resources, and how the establishment of a common biofilm microenvironment could influence their interactions. In this work, we develop an integrative experimental and computational approach to comprehensively assess the metabolic functionality and interactions of probiotics across growth conditions. Our approach combines co-culture assays with genome-scale modelling of metabolism and multivariate data analysis, thus exploiting complementary data- and knowledge-driven systems biology techniques.

To show the advantages of the proposed approach, we apply it to the study of the interactions between two widely used probiotic strains of *Lactobacillus reuteri* and *Saccharomyces boulardii*, characterising their production potential for compounds that can be beneficial to human health. Our results show that these strains can establish a mixed cooperative-antagonistic interaction best explained by competition for shared resources, with an increased individual exchange but an often decreased net production of amino acids and short-chain fatty acids. Overall, our work provides a strategy that can be used to explore microbial metabolic fingerprints of biotechnological interest, capable of capturing multifaceted equilibria even in simple microbial consortia.

## 1. Introduction

Probiotics are live microbes (usually bacteria and yeasts) with beneficial properties for human health. Their precious properties have been recognised by the health industry, medical professionals, and the public, leading to a large range of probiotic products on the market during the last few decades (Kumar et al., 2015). Probiotic microbes are known to produce useful vitamins, digestive, enzymes, essential amino acids, immunomodulatory and antimicrobial metabolites, therefore they can boost human health and protect from gut inflammatory diseases, autoimmune disorders and gastrointestinal infections (De Vrese and Schrezenmeier, 2008). Yet, novel approaches are required to design synthetic probiotic consortia that can overcome the limitations of single-strain formulations (Vázquez-Castellanos et al., 2019).

Microbes are present in nature in two growth modes: the planktonic

mode where the cells swim in the liquid medium and the biofilm mode where cells are attached to each other and/or to a biotic or an abiotic surface, often covered with a protective polysaccharide layer. Usually, the microbes that colonise our intestine form complex biofilm-associated communities, often multispecies (Flemming et al., 2016; Jo et al., 2022). The ability of probiotic microbes to affect our health is linked with their ability to effectively colonise our gut. Therefore, the better their colonisation efficiency, the better their persistence in our gut and subsequently their health effects (Han et al., 2021). For example, the colonisation of *Lactobacillus* species has been shown to inhibit biofilm formation by certain pathogenic bacteria (Salas-Jara et al., 2016).

Besides, metabolic interactions shape the structure of the human gut microbiome and govern how it responds to dietary changes and perturbations (Coyle and Rakoff-Nahoum, 2019). Multi-species cultures have been shown to demonstrate different properties compared to their

\* Corresponding author. School of Computing, Engineering and Digital Technologies, Teesside University, Middlesbrough, United Kingdom.

E-mail address: [c.angione@tees.ac.uk](mailto:c.angione@tees.ac.uk) (C. Angione).

<https://doi.org/10.1016/j.ymben.2023.01.008>

Received 18 June 2022; Received in revised form 13 December 2022; Accepted 21 January 2023

Available online 28 January 2023

1096-7176/© 2023 The Authors. Published by Elsevier Inc. on behalf of International Metabolic Engineering Society. This is an open access article under the CC BY license (<http://creativecommons.org/licenses/by/4.0/>).

single-species planktonic counterparts, as the different species interact with each other and they modify the physiological behaviour and the metabolic output of the culture (Ghosh et al., 2016; Medlock et al., 2018). This has been found to also improve the beneficial health effects of a probiotic supplement, such as its immunomodulatory and antibacterial properties (Chapman et al., 2012; Foligné et al., 2016; Alshaikh et al., 2022). Multi-strain probiotics can more effectively improve host health, provided that the strains do not compete for the same resources or inhibit the growth of other strains (Toscano et al., 2017). For instance, a co-culture study with *Lactobacillus acidophilus*, *Bifidobacterium bifidum* and *S. boulardii* was performed using a complex protein-enriched cereal medium (boza) as substrate, which supported the growth of all three species (Arslan-Tontul and Erbas, 2020). Similar examples of co-cultures of yeast and bacteria for a variety of applications in the food industry and wastewater treatment showed that mixed cultures had better results in these bioprocesses compared to mono-cultures (Jin et al., 2019; Dysvik et al., 2020; Liu et al., 2019). In particular, in a study by Jin et al. the end probiotic product (mango slurry) that was co-fermented by *Lactobacillus plantarum* and *S. cerevisiae* DV10 exhibited higher bioactivity, with more phenolics and antioxidants. Moreover, how biofilms influence the interactions among gut microbiome members is an open question (Salas-Jara et al., 2016).

Among the techniques for exploring microbial interactions, constraint-based genome-scale modelling of metabolism provides a bottom-up approach that fully integrates available biochemical knowledge, can span complex multi-omic networks, and is well suited to explore the biotechnological potential of microbes (Fang et al., 2020; Zampieri et al., 2019; Colarusso et al., 2021; Occhipinti et al., 2018). Such an approach is based on the mathematical formalisation of biochemical reaction stoichiometry and physical conservation laws, which at the steady state permit efficient computation of the reaction fluxes across metabolic pathways. One of the emerging frontiers in this field is the modelling of ecological interactions in microbial and microbe-host communities, with recent studies investigating ecosystems of rising size and diversity (Machado et al., 2021; Basile et al., 2020; Thiele et al., 2020). Notably, this modelling approach offers a platform for experimental data integration and hypothesis testing on a systems level, taking into account multiple objectives (Bauer et al., 2017; Vijayakumar et al., 2018; Zomorodi et al., 2014). For example, genome-scale modelling can be used to analyse the steady-state or dynamic metabolism sustaining biofilm formation and revealed non-intuitive dependencies of biofilm-forming ability in the pathogen *Pseudomonas aeruginosa* (Ribaud et al., 2017; Vital-Lopez et al., 2015). However, scarce attention has been dedicated to the modulation of microbial interactions over changing growth modes and to the contribution that data-driven approaches can offer to their characterisation (Culley et al., 2020; Zhang et al., 2020; Vijayakumar et al., 2020; Antonakoudis et al., 2021; Pio et al., 2022).

This study aims to introduce and test a systematic approach for the characterisation of microbial interactions in multiple growth conditions. As a prototype application, we focused on evaluating the capacity of *L. reuteri* and *S. boulardii* communities to produce metabolites relevant to gut health while also examining their ecological relationship, effectively estimating their potential as a multi-strain probiotic. To this end, we sought to evaluate how metabolic interactions between the selected strains are affected by their growth mode compared to isolated growth. We thus designed and applied an integrated experimental and computational approach that fully characterises metabolic phenotypes in an experimental design space considering strain pairing and growth mode.

*Lactobacillus reuteri* and *Saccharomyces boulardii* are two important probiotic species that are already widely available on the market as health supplements. *L. reuteri* is a Gram-positive bacillus that can produce antimicrobial molecules, such as organic acids, ethanol, and reuterin. Via its antimicrobial activity, *L. reuteri* can inhibit the colonisation of pathogenic microbes and improve the balance of the commensal microbiota composition in the host. Secondly, *L. reuteri* can benefit the

host immune system by reducing the production of pro-inflammatory cytokines while promoting regulatory T-cell development and function. Thirdly, it strengthens the intestinal barrier and decreases microbial translocation from the gut lumen to the tissues (Mu et al., 2018). *S. boulardii* is a yeast that is resistant to the gastric environment and has good viability at low pH. It leads to the improvement of gut barrier function, pathogen competitive exclusion, production of antimicrobial peptides, immune modulation, and trophic effects (Pais et al., 2020).

We performed a collection of microbial cultures for each growth setting by using rich and minimal media, which generated experimental data that we contextualised and interpreted with a combination of constraint-based and multivariate analysis models. In this way, we obtained a comprehensive picture of strain-level metabolic requirements and potential in each condition. Starting from experimental measurements for only six metabolites in the medium, our approach identified genome-scale changes in the metabolic potential of the two strains that well recapitulate independent evidence. Our results also elucidate cross-feeding among the probiotics, recapitulating cross-feeding phenomena confirmed by independent studies and identifying hypothesised ones supporting the establishment of non-trivial interactions between *L. reuteri* and *S. boulardii*, shifting across different degrees of cooperation and competition. Our approach thus provides a basis for integrative multi-strain probiotic development that can be applied to other microbial consortia.

## 2. Materials and Methods

### 2.1. Microbial strains and media

*Lactobacillus reuteri* DSM20016 (DSMZ, Germany) and *Saccharomyces boulardii* (Swiss Bioenergetics, Switzerland) were used in this study. Two different growth media were utilised for microbial cultures: tryptone soya broth (TSB; Oxoid, UK) and M9 minimal medium with 0.4% glucose (Azatian, Kaur, and Latham, 2019). Solid media with 1.5% Bacteriological Agar No1 (Oxoid, UK) were also prepared using the media mentioned above.

### 2.2. Microbial cultures

A single microbial colony from a solid culture was added to 5 mL of liquid medium and the pre-cultures were prepared aerobically at 37 °C for 5–6 h, with agitation at 250 rpm. 100 µL of these pre-cultures (OD<sub>600nm</sub> 1) were added into each tube or well, containing 10 mL (planktonic cultures) or 2 mL (biofilm cultures) of broth, respectively. Samples were collected from the planktonic cultures at 0, 3, and 6 h (mid and late exponential phase) and from the biofilm cultures at 0, 24, and 48 h. The optical density of the cultures was measured at 600 nm by a spectrophotometer (Libra 512, Biochrom, UK). Colony-forming unit (CFU) concentrations in CFU/mL were also calculated by serial dilutions and colony enumerations on solid media after 24–48 h at 37 °C. Finally, biofilm assays were prepared as described previously (Woodward et al., 2000). For the biofilm assays, sterile polystyrene 24-well plates were used, with each well containing 2 mL of broth. At 0 h, each well was inoculated as above and at 24 and 48 h the liquid phase was removed and the biofilms attached to the bottom of the wells were washed three times with sterile water, before being stained with 1% crystal violet for 5 min. Excess dye was washed three times with tap water and the stained biofilms were de-stained by 70% ethanol. The purple colour of the resulting solution was measured at 550 nm by the spectrophotometer. The biomass dry weight was determined by filtering 1 ml samples through 0.45 µm predried, preweighed nitrocellulose membranes (Milipore, Watford, UK), rinsing three times with distilled water and microwaving twice at 650 W for 5 min. All the cultures were prepared in triplicate.

### 2.3. Biochemical measurements

Eight biochemical assay kits (Sigma-Aldrich, UK) were used for the measurement of glucose (product code: MAK013), glycerol (MAK117), succinate (MAK184), acetate (MAK086), ethanol (MAK076), SCFA (SBR00030), L-amino acid (MAK002) and ammonia (AA0100) levels in the culture medium. The planktonic culture samples were centrifuged at 4000×g and the cell-free supernatant was used for the biochemical assays as recommended by the manufacturer. Each biofilm was disrupted within the liquid broth of the well, vortexed for 30 s and centrifuged for 5 min at 12,000 rpm. The supernatant was used for the metabolic assays. For colorimetric assays, a Biotek ELX 808 multiwell plate reader (Lonza, Switzerland) was used. All the measurements were made in triplicate.

### 2.4. Genome-scale model reconstruction

Although a manually curated genome-scale metabolic model (GSMM) for *L. reuteri* JCM 1112, Lreuteri\_530, was previously published (Kristjansdottir et al., 2019), this was found to have a high percentage of flux-inconsistent reactions (Supplementary Table 1). We thus generated a new GSMM for *L. reuteri* DSM20016 exploiting recent advances in automated GSMM reconstruction (Mendoza et al., 2019), while also leveraging previous curation efforts. An updated proteome sequence for *L. reuteri* DSM20016 was retrieved at the NCBI portal under accession number 166843. This was used in the GSMM reconstruction through CarveMe v1.5.1 (Machado et al., 2018) in Python 3.6. Compared to other GSMM reconstruction tools, CarveMe has been shown to generate models with a higher reaction set similarity to manually curated networks and a lower content in incomplete pathways with dead-end metabolites (Mendoza et al., 2019). Additionally, CarveMe allows the definition of custom metabolic universes used for model creation. As Lreuteri\_530 was developed within the BiGG namespace (King et al., 2016), we therefore expanded the native gram-positive universe with its reactions and metabolites. This allowed us to use a larger set of network components that more likely capture *L. reuteri* metabolism. Finally, upon draft reconstruction, the model was gap-filled for growth on the M9 medium supplemented with biotin and thiamine, requiring that the import and export of sampled metabolites matched experimental observations, through the –hard argument. Non-growth-associated maintenance energy requirement of Lreuteri\_530 was integrated into our newly built model as a lower bound on the ATPM reaction corresponding to 0.36 mmol/g/h.

The obtained GSMM was quality-controlled through a series of functionality tests, benchmarking against Lreuteri\_530 and a model of *L. reuteri* F275 JCM 1112 previously automatically reconstructed via a different approach (Magnúsdóttir et al., 2017) (Supplementary Table 1). Our newly generated model incorporates 54% of the reactions and 69% of the metabolites present in the curated model, while almost doubling the number of reactions and introducing 43% as many metabolites. Further, our model has only 2.4% of flux inconsistent reactions, against 35.4% of the curated model, and correctly passes the other functionality tests (Supplementary Table 1). All the tests were performed by using the COBRA toolbox 3.0.6 (Heirendt et al., 2019) with CPLEX 12.8 as a mathematical programming solver. To characterise the differences between our model and Lreuteri\_530 in terms of functional subsystems, we mapped BiGG reaction identifiers to those of the ModelSEED database (Seaver et al., 2021) via MetaNetX (Moretti et al., 2021). Our model results expanded in a number of metabolic functions, especially those related to carbohydrates, amino acids, and membrane transport. Methionine biosynthesis and arginine, ornithine, and isoleucine degradation are among the pathways with most introduced annotations, which also comprise thiamin and cholate biosynthesis and purine and pyrimidine conversions. Quantitative improvements in terms of reaction class, subclass, and pathway annotation are provided in Supplementary Fig. 1.

To have GSMMs within the same namespace, and because eukaryotic

organisms are in general more complex to accurately model, for *S. boulardii* we adopted iMM904, a curated and experimentally validated *Saccharomyces cerevisiae* GSMM (Mo et al., 2009). Current genomic evidence supports that these organisms are in fact two strains of the *cerevisiae* species, with recent comparative analysis showing that the probiotic yeast is taxonomically close to wine strains of *S. cerevisiae* and possesses the same genes involved in biofilm formation (Khatri et al., 2017). In this way, we secured a physiologically meaningful model for the yeast.

### 2.5. Flux sampling

Starting from the biochemical measurements, the corresponding metabolite production and consumption rates  $q$  were calculated by using the following relation:

$$\frac{dN}{dt} = qX(t), \quad (1)$$

where  $N$  represents the metabolite concentrations and  $X$  the biomass at time  $t$ . Standard deviations obtained from triplicate measurements were propagated to determine exchange rate errors  $\Delta q$ . The obtained values were converted to mmol/g<sub>DW</sub>/h and used to constrain the GSMMs by setting  $q \pm 3 \cdot \Delta q$  as upper and lower bounds for each metabolite's exchange rate. Growth rate constraints were set analogously as  $\mu \pm 3 \cdot \Delta\mu$ , where  $\mu$  was determined from logarithmic interpolations of OD<sub>600</sub> and OD<sub>550</sub> measurements for the planktonic and biofilm cultures, respectively, and its error  $\Delta\mu$  was obtained by propagation. For all the metabolites in the medium without experimental measurements, we set 10 mmol/g<sub>DW</sub>/h as an uptake rate bound to avoid unrealistically large flux distributions.

To explore the space of feasible metabolic states allowed by the integration of biochemical, culture type and growth mode constraints, we employed metabolic expectation propagation (MEP) (Braunstein et al., 2017). This method analytically approximates a flux distribution as a multivariate truncated Gaussian and allows efficient computation of its parameters (mean and variance) through the expectation propagation algorithm. Moreover, in contrast to traditional flux sampling methods, empirical evidence can be explicitly taken into account by MEP by matching the experimentally measured mean and variance of any flux with the corresponding posterior distributions. We therefore provided the algorithm with experimental information regarding glucose, glycerol, ammonia, ethanol, acetate, succinate, and growth, selecting a more relevant flux configuration subspace. Upon obtaining the flux distribution parameters, we sampled 1000 genome-scale flux configurations for each strain through a minimax tilting method (Botev, 2017).

Using sampled flux solutions, growth-normalised fluxes were defined as the ratio between their value and the cellular growth rate in the respective condition. Growth rate being equal, growth-normalised fluxes represent the biochemical transformation rates necessary for maintaining such growth rate.

### 2.6. Modelling biofilm formation

To explicitly account for the metabolic rewiring associated with biofilm formation, we modified the biomass pseudo-reaction of both organisms with an approach adopted also in previous studies (Ribaudou et al., 2017). We assumed that biomass accumulation could be divided into a cell-growth-associated and a biofilm-associated component, as follows:

$$(1 - \alpha) \sum_i c_i^{\text{growth}} + \alpha \sum_j c_j^{\text{biofilm}} \rightarrow \text{environment}, \quad (2)$$

where  $c_i^{\text{growth}}$  and  $c_j^{\text{biofilm}}$  represent the coefficients of compounds linked to cell growth and biofilm formation, respectively, whereas  $\alpha$  represents

the fraction of biofilm-forming biomass over total biomass. Having  $\alpha$  fixed, the effect is thus a rescaling of the percent biomass contribution for all compounds natively present in the biomass pseudo-reaction by a factor  $(1 - \alpha)$ , with the additional term expressing the fractional contribution of the extracellular matrix components weighted by their molecular mass.

In general, the biofilm matrix is largely composed of extracellular biomass, with minor fractions of microbial cells (Flemming et al., 2016). In our work, we assumed that around two-thirds of the total biomass is directed toward extracellular matrix formation and thus set  $\alpha = 0.65$ , following previous studies (Ribaudou et al., 2017). Coefficients  $c_j^{\text{biofilm}}$  were established based on the available evidence on strain-dependent biofilm matrix composition and the corresponding molecular weights for these components. The mechanisms for *L. reuteri* biofilm development have been characterised *in vivo*, identifying some key genes whose products are secreted depending on the development stage (Frese et al., 2013; Terraf et al., 2016). Specifically, a Fap1-like protein has been identified as necessary for the initial adherence to a surface, while LysM/YG proteins are responsible for the formation of cell aggregates and macro-colony development (Frese et al., 2013). To best reproduce the metabolic requirements associated with the production and secretion of these proteins, including the serine-rich Fap1-like protein, we retrieved their sequence and assumed their amino acid proportion as the coefficients in our biomass pseudo-reaction, appropriately rescaled by their molecular weight. The energetic requirements for amino acid polymerisation were assumed as 2.306 ATP/molecule, setting the corresponding coefficients accordingly (Kaleta et al., 2013).

In *S. cerevisiae*, the extracellular biofilm matrix is mainly made up of glucose, mannose, and galactose (Beauvais et al., 2009; Faria-Oliveira et al., 2015). Based on previous results of genomic comparisons, we assumed similar biofilm formation mechanisms in *S. boulardii* (Khatri et al., 2017). We thus defined the extracellular matrix as comprised by the polysaccharides of glucose and mannose present in the model, including 1,3- $\beta$ -D-glucan, glycogen, and mannan, together with galactose in uniform proportions.

## 2.7. Microbial community modelling

Microbial community GSMs representing the mixed cultures were created through the createMultipleSpeciesModel function in the COBRA toolbox (Heirendt et al., 2019). The result was the creation of a common extracellular compartment where the individual GSMs are encapsulated and share boundary metabolite exchanges with the environment, effectively allowing the simulation of cross-feeding and nutrient competition. To simulate a metabolic activity reproducing growth patterns observed experimentally, we introduced a community biomass pseudo-reaction, defined as follows:



here,  $\mu_{LR}$  and  $\mu_{SB}$  denote the flux through the individual biomass pseudo-reactions of *L. reuteri* and *S. boulardii*, which may include both cellular and biofilm components depending on the culture mode. These rates were weighted by the strain relative abundances  $a_{LR}$  and  $a_{SB}$ , calculated as the average CFU fraction for each strain over time. Biochemical constraints were set in the same way as for the mono-culture simulations on the global metabolite exchanges and on the community growth rate.

## 2.8. Multivariate flux analysis

To explore fluxomic profiles obtained by metabolic modelling and extract key information, we employed principal component analysis (PCA) via the Matlab pca function. Prior to performing PCA, flux profiles  $\mathbf{X}$  were standardised to have null mean and unitary standard deviation through the Matlab zscore function.

To analyse the relationship between experimental factors and indi-

vidual strain metabolism, we used an approach that extends both correspondence analysis and partial least squares correlation, termed partial least squares correspondence analysis (PLSCA) (Beaton et al., 2016). Given two data matrices  $\mathbf{X}$  and  $\mathbf{Y}$  representing the flux profiles and the experimental factors respectively, pre-processed so that they have zero mean and unitary norm, we define  $\mathbf{R} = \mathbf{X}^T \mathbf{Y}$ . PLSCA determines two sets of latent variables of maximal covariance by the generalised singular value decomposition, as follows:

$$\mathbf{R} = \mathbf{U} \mathbf{\Delta} \mathbf{V}^T \quad \text{with} \quad \mathbf{U}^T \mathbf{W}_X \mathbf{U} = \mathbf{I} = \mathbf{V}^T \mathbf{W}_Y \mathbf{V}. \quad (4)$$

here,  $\mathbf{U}$  and  $\mathbf{V}$  are the matrices of the left and right singular vectors, respectively,  $\mathbf{\Delta}$  is a diagonal matrix containing the singular values, while  $\mathbf{W}_X$  and  $\mathbf{W}_Y$  are diagonal matrices weighting the occurrence of categorical variables assuming that rare occurrences are more informative than frequent ones. Akin to PCA, PLSCA projects the two data matrices onto a latent space described by orthogonal axes of decreasing covariance. As biochemical reaction fluxes constitute quantitative features, we processed them through the Escofier transformation before using PLSCA (Beaton et al., 2016). Such transformation takes a continuous, centred and scaled feature  $x$  and expresses it as two new variables obtained as  $\frac{1-x}{2}$  and  $\frac{1+x}{2}$ . PLSCA and the relative data pre-processing were performed with the TExPosition package v2.6.10.1 (Beaton et al., 2014).

Finally, hierarchical clustering was performed using Euclidean distances and complete linkage through the Matlab linkage and dendrogram functions. For this analysis, exchange fluxes were rescaled by the maximum absolute exchange for each metabolite, in order to obtain values between  $-1$  and  $1$ .

All the analyses were carried out in Matlab R2017b and R 3.5.0.

## 2.9. Statistical analysis

Statistical comparison of experimentally measured metabolic differences between cultures was performed using unpaired t-tests. Comparison of metabolic flux distributions sampled *in silico* was instead carried out by Wilcoxon rank-sum tests, controlling the false discovery rate by adjusting the p-values with the Benjamini-Hochberg correction (Benjamini and Hochberg, 1995).

To evaluate the robustness of PLSCA principal components, we resorted to an eigenvalue-based randomisation test as described previously (Peres-Neto et al., 2005). In brief, the test assumes  $k$  random permutations of each feature independently among the samples, obtaining a new data matrix  $\mathbf{X}'$  upon any permutation. For each of them, PLSCA of the shuffled data was repeated and the latent variable variances  $\lambda$ , i.e., the eigenvalues of the covariance matrix of  $\mathbf{X}'$ , were recorded. The probability of obtaining a certain latent variable by chance was calculated by:

$$p = \frac{|\{\mathbf{X}' \in \widehat{\mathbf{X}} : \lambda(\mathbf{X}') \geq \lambda(\mathbf{X})\}| + 1}{k + 1}. \quad (5)$$

In our case, the number of permutations was  $k = 999$ . This test thus verified that the model had identified meaningful latent variables.

## 3. Results

### 3.1. Exploration of the proposed multi-strain probiotic potential

To characterise the metabolic interactions in the multi-strain probiotic composed of *L. reuteri* and *S. boulardii*, we designed a two-factor strategy considering: (i) the capacity to form biofilms; and (ii) the interaction arising from sharing the same growth environment. We set up culture experiments where the strains were grown either in a planktonic or a biofilm mode and either in isolation or co-growth with the other strain (Fig. 1). In each of the resulting four cases, the strains were cultivated both in simple (M9) and complex media (TSB) to test the response to different levels of nutrient availability. Growth and activity

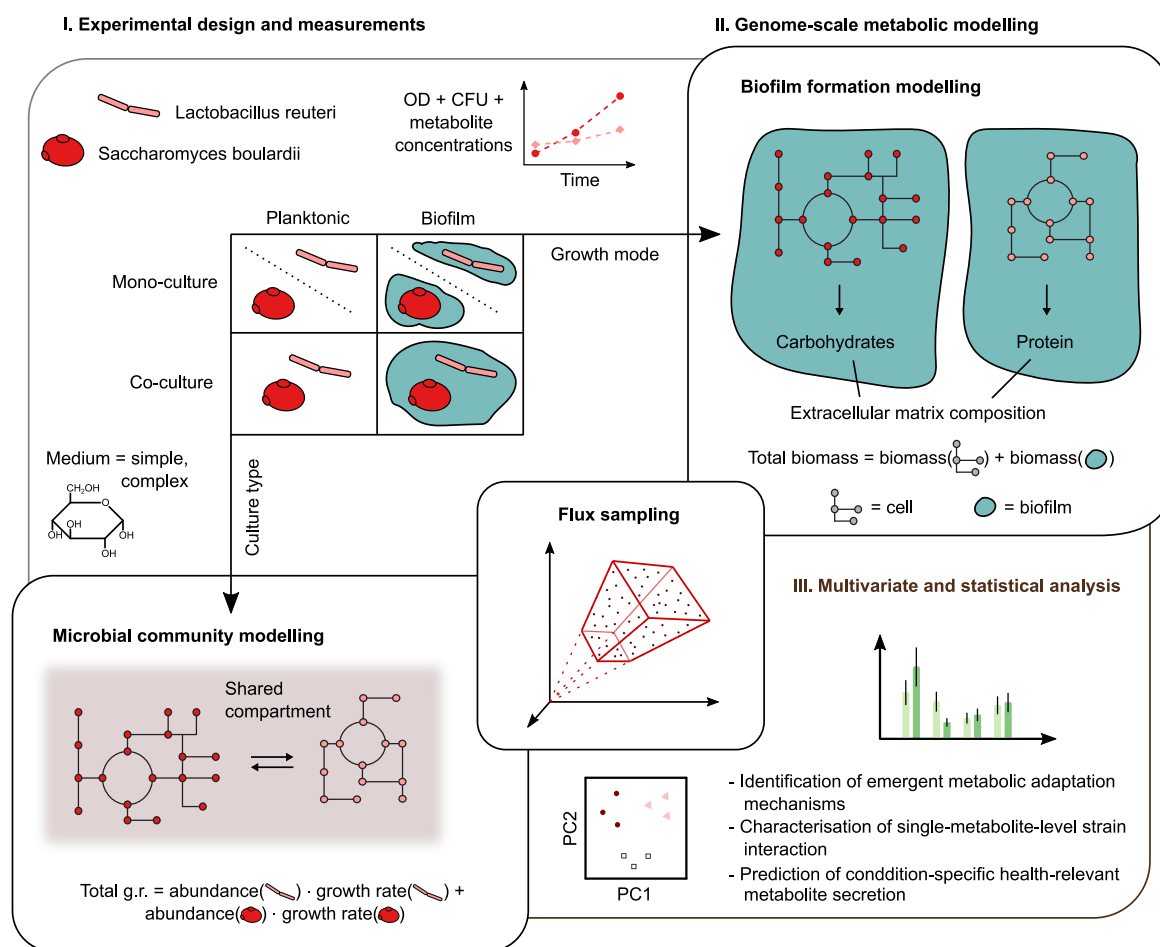


**Fig. 1.** Schematic diagram of the experimental and computational design of the study. Starting from two isolated strains of *L. reuteri* and *S. boulardii*, we experimentally characterised their growth and metabolic behaviour across culture types (mono- and co-cultures) and growth modes (planktonic and biofilm), both in simple and complex medium. Next, we expanded the observed metabolic activity up to the genome-scale using constrained-based models of metabolism for the two strains and dedicated modelling strategies for microbial communities and biofilm development. To obtain a comprehensive picture of the metabolic potential in each condition, we used flux sampling and fully explored the achievable metabolic states. Given their high dimensionality and complexity, these were subsequently analysed through multivariate and statistical modelling approaches.

for each culture were monitored over time based on optical density, number of CFU and concentrations for a set of relevant metabolites (see Materials and Methods).

To fully reconstruct and interpret the metabolic behaviour of the strains in each condition, we devised an *in silico* approach for charting all axes of the biological space explored. A GSMM for *L. reuteri* was assembled starting from its proteome sequence, spanning 1390 reactions, 942 metabolites, and 530 genes (see Materials and Methods for details). The model incorporates biochemical transformations for the production of reuterin and 1,3-propanediol, which are among the hallmark products of this organism, and several molecules relevant to gut physiology like vitamins and amino acids, for a total of 177 exchange reactions. For *S. boulardii*, an extensively validated yeast model was used based on recent genomic evidence (Mo et al., 2009; Khatri et al., 2017). This model encompasses 1577 reactions, 1226 metabolites, and 905 genes, with a curated set of secretion pathways resulting in 164 exchange reactions. Further, manually reviewed cofactor biosynthetic pathways are present, including quinone, beta-alanine, and riboflavin. By using such GSMMs, we sampled the space of metabolic reaction flux configurations that were consistent with observations from the cultures. Measured growth and metabolite concentration change rates were used to constrain the models, shaping the multidimensional flux space of the networks accordingly. Additionally, to reproduce the different growth settings, we devised *ad hoc* constraints based on the definition of

alternative biomass pseudo-reactions. In this way, we modelled the growth modes and the culture types in a condition-specific fashion.

In general, the biofilm matrix composition varies from organism to organism. For example, *L. reuteri* makes colonies composed of cell aggregates through the secretion of peptidic anchors (Frese et al., 2013; Terraf et al., 2016) while *S. boulardii* mainly exploits glucose, mannose, and galactose polymers (Beauvais et al., 2009). To account for appropriate biofilm compositions and associated metabolic costs, we modified the biomass pseudo-reaction in the GSMMs of the individual strains based on the evidence provided by these studies (see Materials and Methods for details). The microbial communities were instead modelled by defining an outer shared compartment including the metabolic networks of the individual strains. Such an approach allows one to unambiguously determine the metabolic inputs and outputs for each member of the community, which is essential for understanding the effects of each biological parameter on their activity. To formalise the relationship between the strains, we constrained the community GSMM with the experimentally observed growth and metabolite dynamics. To this end, we defined a community biomass pseudo-reaction whose flux was required to lie in the experimental range and where the contribution to the total growth of each strain was set as the relative abundance in terms of CFU counts (see Materials and Methods). The metabolite concentration change rates were used to constrain the boundaries of the system, namely the exchange rates in the shared compartment.

In all the conditions, we therefore used a specific network structure and parametrisation while exploiting the experimental data to focus on the relevant solution subspace. Such an approach had the purpose of yielding the ranges of metabolic phenotypes for the two strains that are both allowed by the observations and consistent with biochemical network knowledge. The obtained space of achievable metabolic fluxes was characterised in full to estimate the unobserved metabolic potential.

### 3.2. Ecological interactions between *L. reuteri* and *S. boulardii*

Overall, *L. reuteri* grew better and faster planktonically by 6 h than *S. boulardii* in rich medium and similarly in minimal media, however *S. boulardii* formed better biofilms by 48 h (Fig. 2A). Moreover, the type of medium had a more marked effect on growth across the biofilm cultures than the planktonic ones, consistently with an elevated metabolic cost necessary for the establishment of biofilm colonies. It was also observed that CFU concentration at the final time point significantly changes when growing the strains together (Fig. 2B). In particular, *L. reuteri* planktonic growth was drastically reduced in the mixed cultures, while that of *S. boulardii* was positively affected. In biofilms, the same trend occurred even with a less pronounced inhibition of *L. reuteri*. When performing these measurements in anaerobic conditions, *L. reuteri* showed a faster growth and *S. boulardii* showed a slower growth, which resulted in a slower growth also for the mixed cultures (Supplementary Fig. 2). CFU counts confirmed the same trends in anaerobiosis, highlighting again the suppression of *L. reuteri* (Supplementary Fig. 2).

Multiple mechanisms may in principle underlie such patterns (Fig. 2C). Firstly, a more efficient nutrient utilisation might allow the yeast to thrive at the expense of the lactobacillus. Secondly, *S. boulardii* could benefit from some of the metabolites secreted by *L. reuteri* (e.g.

sugars) or the latter species could be harmed by some of the former's byproducts. For instance, Ponomarova et al. suggested a potential mechanism by which yeast cells and lactic acid bacteria can interact with each other when they are in the same culture (Ponomarova et al., 2017). *S. cerevisiae* was found to secrete a pool of amino acids that were taken up by the lactic acid bacteria and helped them survive. In return, if lactose was present in the medium, the lactic acid bacteria could break it down to galactose and glucose, making it accessible to the yeast. In addition, Jarosz et al. suggested a prion-based mechanism of communication between yeast and bacterial cells in co-culture (Jarosz et al., 2014). In that case, the bacteria induced a prion that made the yeast cells produce less ethanol, allowing the bacteria to survive and flourish in the mixed culture. Alternatively, the secretion of proteins or glycoproteins with antimicrobial effects, termed mycocins, might contribute to *L. reuteri* suppression (Rima et al., 2012). Finally, growth-coupled ion exchange or organic acid production might trigger a pH reduction, which can affect *L. reuteri* metabolism on multiple functional levels (Lee et al., 2008).

At the metabolic level, several differences were observed between mono- and mixed cultures, as shown in Fig. 3. For example, nearly seven times more ammonia was consumed by 6 h in M9 mixed cultures than in the corresponding mono-cultures. In addition, about two times more acetate and succinate were formed in the mixed planktonic and biofilm cultures. Statistical values are shown in Fig. 3D. Moreover, in anaerobiosis, acetate accumulated in the medium in larger amounts (Supplementary Fig. 2). Acetate and succinate are metabolites that can have positive effects on human health. Acetate is a short-chain fatty acid (SCFA) that has been shown to reduce inflammation in the gut and affect the gut-brain axis, while succinate availability is important for all the metabolic pathways that are interlinked with the TCA cycle, including

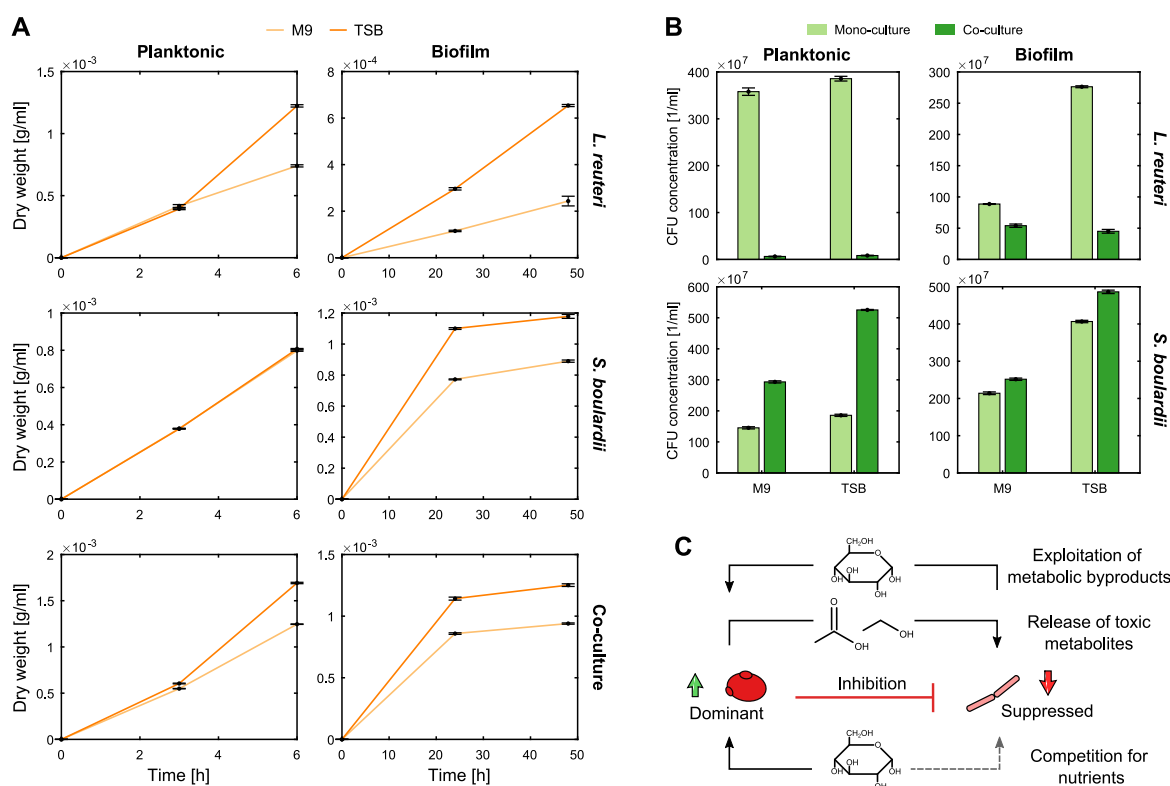


**Fig. 2.** The effect of co-culture on the growth of the individual strains. A. Dry weight dynamics for *L. reuteri* (top), *S. boulardii* (middle), and their mixed culture (bottom), each grown in planktonic (left) and biofilm mode (right). Planktonic cultures were sampled at 0, 3, and 6 h post-inoculation, while biofilm cultures were sampled at 0, 24, and 48 h post-inoculation. All measures were done in three biological replicates. B. Comparison of the final CFU concentration in pure and mixed cultures for *L. reuteri* (top) and *S. boulardii* (bottom) when grown in planktonic (left) and biofilm mode (right). All measures were done in three biological replicates. C. Potential mechanisms underlying the growth patterns of the two strains, where *S. boulardii* results as a beneficiary of mixed growth while *L. reuteri* is suppressed. The former may have a more effective resource utilisation and potentially inhibit the partner through secreting compounds with a toxic effect or lowering pH.

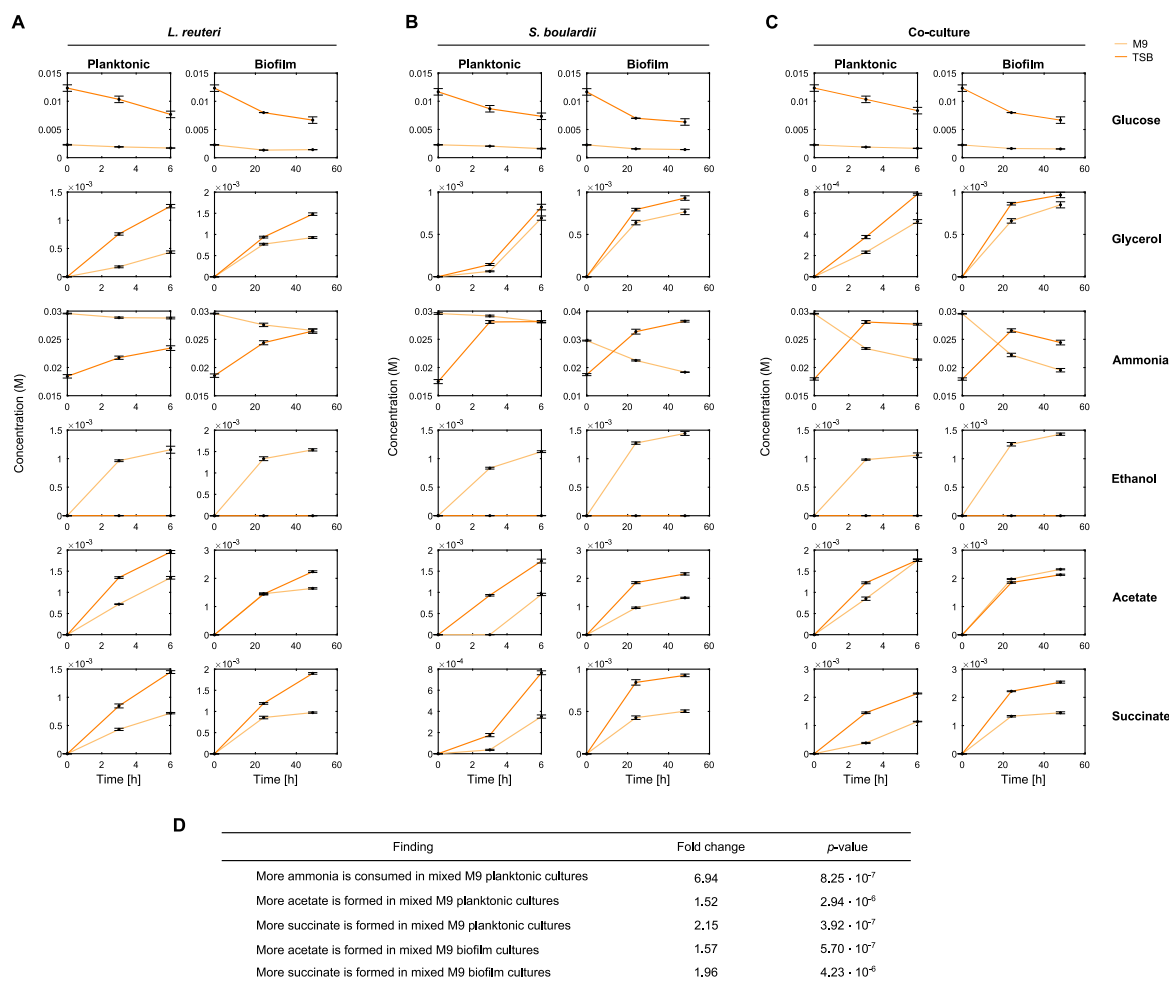


**Fig. 3.** Concentration of monitored metabolites over time across the cultures. A. *L. reuteri* cultures. B. *S. boulardii* cultures. C. Mixed cultures. Planktonic cultures were sampled at 0, 3, and 6 h post-inoculation, while biofilm cultures were sampled at 0, 24, and 48 h post-inoculation. N = 3, where N is the number of biological replicates. D. Key metabolic differences between mixed and mono-cultures were assessed by using unpaired t-tests.

the metabolism of carbohydrates, amino acids, fatty acids, cholesterol, and heme and is also involved in immune signalling (Dalle et al., 2019; Mills and O’Neill, 2014).

### 3.3. Assessing the genome-scale metabolic potential of the multi-strain communities

The biochemical data shown above indicate increased production of acetate and succinate in the lactobacillus-yeast consortium, yet they embrace a limited set of metabolites. To comprehensively estimate the metabolic potential that was not directly measured, we employed constraint-based modelling as described above.

GSMs account for a large range of metabolites that can be exchanged with the environment and microbial partners, including amino acids, sugars, nucleotides, vitamins, and fatty acids. By considering consumption/production potential estimates for such a range of metabolites, marked differences between the cultures emerge. Fig. 4A shows a PCA representation of the cultures in terms of the corresponding metabolic exchanges. While using only experimentally measured exchanges the cultures appear broadly distinguishable based on the medium, when integrating the *in silico* estimates the picture drastically changes. Co-cultures in complex medium display an emergent metabolic behaviour, visible as a gap separating them from the respective single cultures, consistent with a broad metabolic rewiring associated with the established biotic interaction. Such a behaviour has been previously

observed in co-culture studies (Medlock et al., 2018) and reveals that even pairwise co-growth can present complex interactions. While here it is observed for *in silico* predictions and might not precisely reflect the real metabolic rewiring, it is thus reasonable to assume that, on a broad level, this pattern takes place *in vitro* as well. Moreover, the role of individual metabolites appears better defined when accounting for genome-scale variability. For instance, a larger ethanol release results as more clearly associated with the simple medium, while succinate production appears better associated with the complex medium compared to glycerol and acetate.

As regards metabolites relevant to the gut microbiota, it was observed that different conditions lead to increased exchange potential for different beneficial microbial metabolites (Fig. 4B). For example, our models predicted a secretion of biotin from *S. boulardii*, which decreases in the biofilm mode when utilising the minimal medium and increases with the complex medium. Analogously, a multi-strain environment is associated with a decrease in biotin production in the minimal medium, whereas the opposite trend is observed in the complex medium. Concomitantly, various changes in amino acid exchanges characterise the different growth modes. In M9, the amino acids L-valine, L-isoleucine, L-methionine and L-histidine, as well as the short-chain fatty acids formate, L-lactate and D-lactate are more highly produced in mono-cultures, while L-serine and L-lysine are more highly produced in mixed cultures. In mixed cultures, we also see a higher production of glycine, isobutyric, isovaleric acid, the antimicrobial compound reuterin

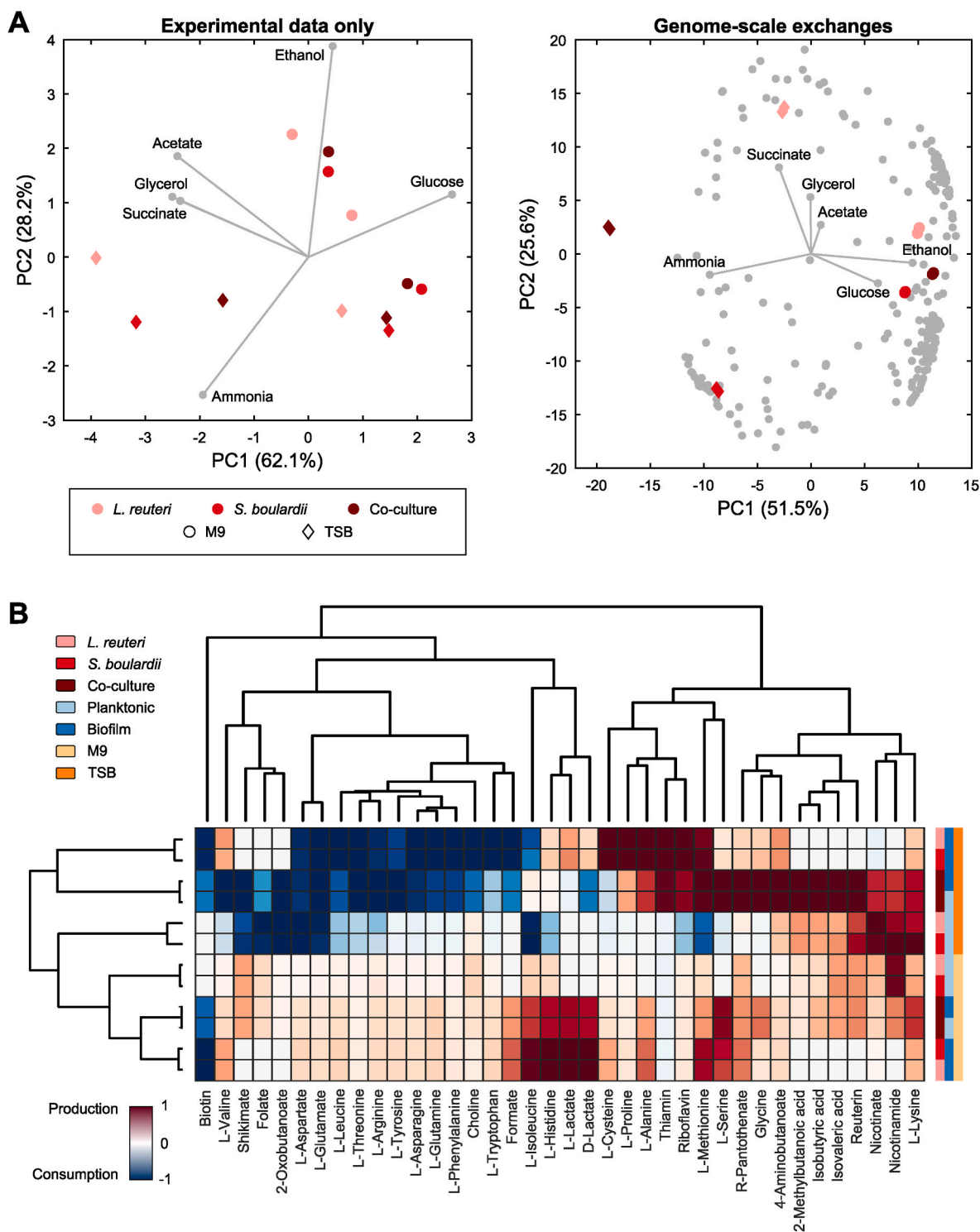


**Fig. 4.** Global metabolic exchange potential reconstructed *in silico*. A. Principal component analysis (PCA) of average measured (left) and *in silico* inferred (right) metabolic exchange rates for the twelve cultures. Variable loadings were rescaled to fit the plot so that the maximum loading distance and the maximum data point distance from the origin were equal. B. Agglomerative clustering characterising the average exchange rates for a range of amino acids, vitamins and short-chain fatty acids. Values were rescaled by dividing exchange rates by the maximum rate obtained for each metabolite.

and nicotinamide (vitamin B3 or niacin). Nicotinamide is more highly produced in the planktonic state. Shikimate, an amino acid precursor, is overproduced in mixed cultures and planktonic mono-cultures. In TSB, six metabolites (L-valine, L-lactate, L-cysteine, L-proline, L-alanine and riboflavin - or vitamin B2) had increased exchange potential in mono-cultures, while eleven others (L-serine, R-pantothenate - or vitamin B5, Glycine, 4-aminobutanoate, 2-methylbutanoic acid, isobutyric acid,

isovaleric acid, reuterin, nicotinate (a vitamin B3 precursor), nicotinamide and L-lysine) had increased exchange potential in mixed cultures.

To evaluate the confidence in model predictions while also getting a comprehensive recapitulation of the above results, we measured total amino acid secretion rates across conditions. Fig. 5 shows that, although model fluxes tend to be inflated with respect to experimental values, trends were correctly captured, such as, in particular, the decrease in

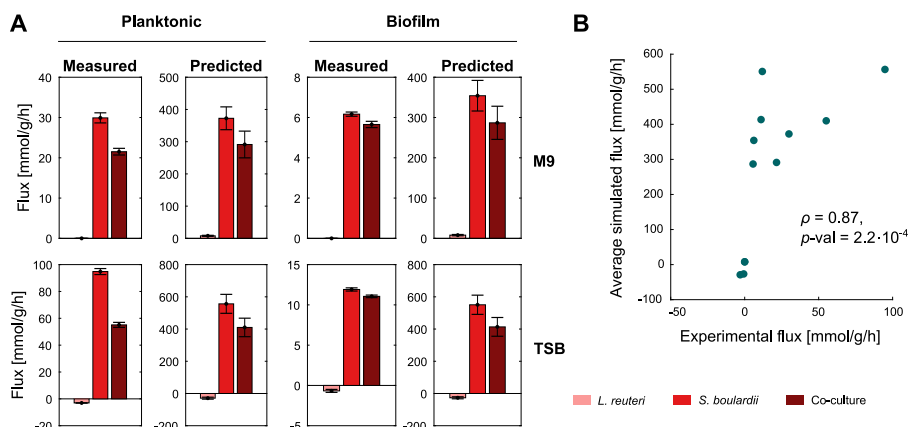


**Fig. 5.** Model validation focusing on amino acid production. A. Comparison between experimentally measured and computationally predicted total amino acid exchange rates across all the conditions. B. Global relationship between experimentally measured and computationally predicted total amino acid exchange rates, where  $\rho$  denotes the Spearman correlation coefficient.

total amino acid production rates in mixed cultures compared with *S. boulardii*. Thus, it emerges that *S. boulardii* produced amino acids at the highest rate in all the conditions, but also that biofilms are associated with a strong reduction in such rates. Measurement of total SCFA production rates allowed us to verify a positive correlation with GSMM estimates also there, even though uncertainty over the precise detected metabolite identity makes it more difficult to fully evaluate these results (Supplementary Fig. 3).

### 3.4. Inferring strain-specific response to varying growth conditions

We next sought to disclose the metabolic exchange trends that characterise the individual strains across conditions, and whether such trends universally correlate with any of the experimental design axes considered. An advantage of our GSMM approach is that even when modelling multi-strain communities the behaviour of the individual members can be directly obtained for free. Each member is in fact embedded in a compartment with well-defined transport reactions, which are distinct from the global system boundary. Thus, we applied PLSCA (Beaton et al., 2016), a multivariate analysis technique that extrapolates the correlation between two sets of variables by extracting the shared variance. In our case, we focused on the relation between the

strain-level metabolic exchange fluxes and the factor set including strain, medium, culture type and growth mode. To better capture the metabolic mechanisms underlying these parameters, we rescaled the fluxes by the growth rate in the corresponding condition, thus obtaining growth-normalised metabolic fluxes for each exchanged compound.

In Fig. 6A, it can be observed that strain and medium type are the parameters that have the strongest effect on growth-normalised metabolite exchanges, given that they are localised the most distant from the origin. Along with a decreasing effect strength, these are followed by the type of culture (mono- or co-culture) and then by the growth mode (biofilm, planktonic). This was expected as different species have different metabolic capabilities, while medium composition (rich, poor) directly affects the nutrients that can be absorbed and consequently the end products that can be exported. Although the specific constraints used here could have potentially inflated its contribution compared to the other parameters (consult Materials and Methods for details), the medium composition is thus reasonably among those with the stronger effect. Interestingly, the type of culture had a stronger effect than the growth mode, which highlights that the ecological interaction between the two species had a significant effect on their metabolic output and reflects the emergent behaviour shown above (Fig. 4A). Among the compounds whose exchange most covaries with

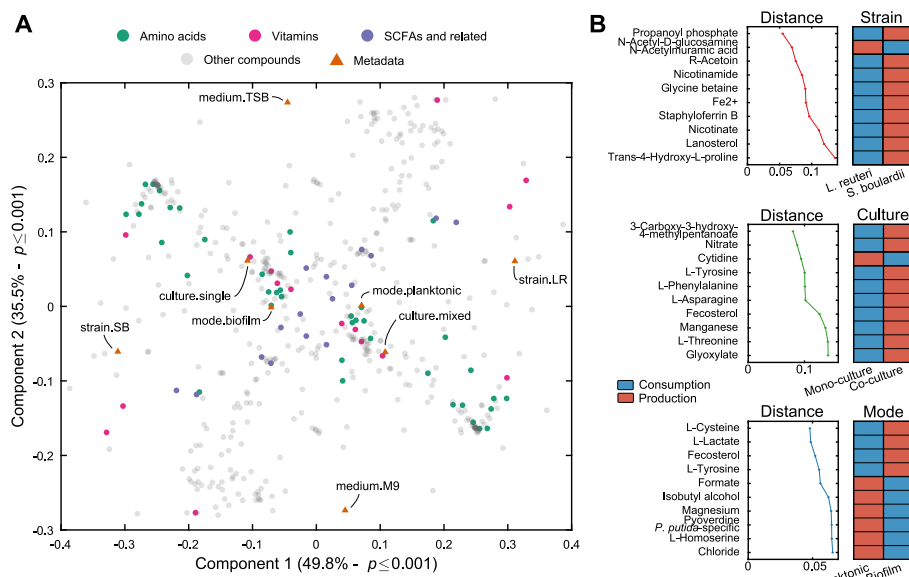


**Fig. 6.** Strain-level trends in growth-normalised exchange fluxes. A. Partial least squares correspondence analysis (PLSCA) capturing relationships between the GSMM-generated growth-normalised metabolic exchanges and experimental factors. The distance from the origin of each dot indicates the contribution to the total covariance of the corresponding flux/parameter, while dot proximity reflects the correlation of respective fluxes/parameters. Fluxes are assigned two dots each, representing values above and below average (see Materials and Methods for details). B. Exchange regimes associated with the experimental factors, for the metabolites that are most highly correlated with each shown factor.

experimental factors are vitamins including biotin, folate, niacin, and nicotinamide, while several amino acids and other vitamins appear associated with the growth mode and culture type. In contrast, SCFAs and related compounds tend to be less associated with specific parameters.

Furthermore, Fig. 6B shows the metabolites whose exchange is most correlated with each parameter pair and in which direction. *S. bouldardii* metabolic activity is generally associated with a higher production of several metabolites, which *L. reuteri* tends to consume or produce in lower amounts. The only exception is N-acetylmuramic acid, which is a bacterial cell wall component. The remaining metabolites include propanoyl phosphate (SCFA derivative), nicotinamide (vitamin B3), iron and a siderophore, staphyloferrin B, lanosterol, a steroid precursor, and trans-4-hydroxy-L-proline, an inhibitor of proline catalysis. The

same picture is seen for mono-vs co-culture, as most metabolites that are most highly correlated with this parameter pair are produced in co-cultures with the exception of cytidine, an RNA component. The remaining metabolites include many amino acids, fecosterol (a fungal cell wall component) and glyoxylate which is an intermediate of the glyoxylate cycle that allows the conversion of fatty acids to carbohydrates. Finally, some amino acids are produced by cells in biofilm mode and consumed by planktonic cells, while other amino acids have the opposite trend. Regarding SCFA, L-lactate is formed by biofilm-associated cells, while formate is produced by planktonic cells.

Finally, we inspected more closely the differences between growth-normalised exchanges in mono- and co-cultures to better evaluate the impact of community establishment and hypothesise more detailed interaction mechanisms. In Fig. 7, it can be seen that numerous health-

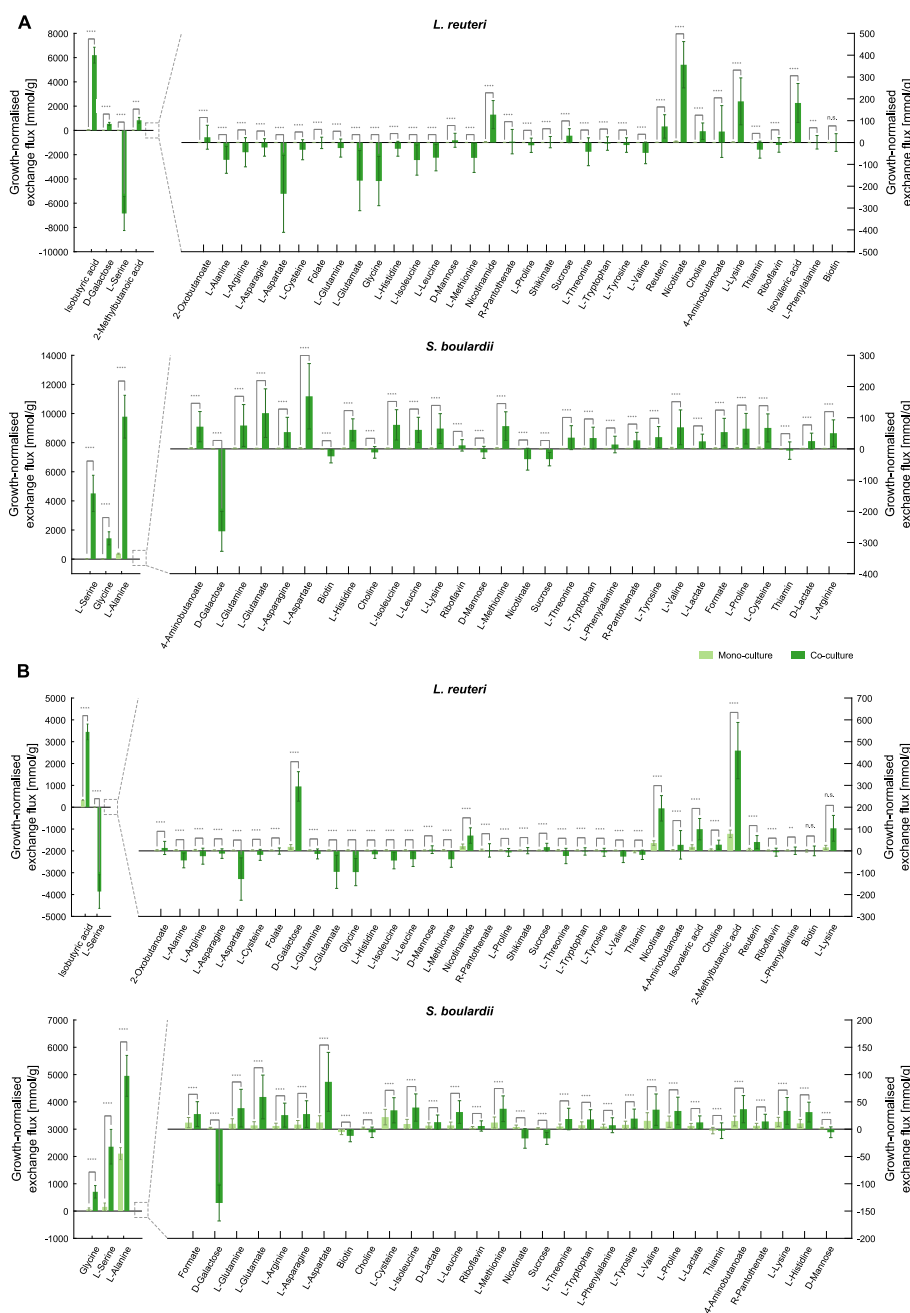


Fig. 7. Strain-specific growth-normalised metabolic fluxes in mono- and co-culture with simple medium for a set of key amino acids, sugars, and vitamins. A. Comparison between the growth-normalised metabolic fluxes of *L. reuteri* and *S. bouldardii* when growing in planktonic mode. B. Comparison between the growth-normalised metabolic fluxes of *L. reuteri* and *S. bouldardii* when growing in biofilm mode.

relevant compounds are more highly produced in co-cultures than mono-cultures when normalising over the growth rate. This observation suggests that, despite a decreased total amino acid production (Fig. 5 and Supplementary Fig. 3), these may in reality be exchanged at large rates by the microbes when growing together. Widespread increased and decreased metabolic efficiency, defined as a reduced or intensified metabolite production per unit of growth, respectively, was previously observed in pairwise co-cultures of gut microbes also including *Lactobacillus* strains (Medlock et al., 2018). Moreover, in the same study, increased efficiency was enriched in microbe pairs having positive interactions. Here, *L. reuteri* and *S. boulardii* display a negative interaction characterised by a suppressed growth of the former. Thus, it is not unreasonable that growth-normalised exchanges point to reduced metabolic efficiency.

Additionally, higher assimilation of amino acids by *L. reuteri* in mixed cultures suggests a mutually beneficial cross-feeding with *S. boulardii*, as observed previously between *S. cerevisiae* and lactic acid bacteria (Ponomarova et al., 2017). Although these strains differ from those considered here, this mechanism could also explain the growth trends observed for our strains. This explanation would be particularly relevant in the case of biofilm communities, given that *L. reuteri* biofilms are predominantly protein-based, as found by previous studies and implemented in our model, and more elevated assimilation of amino acids was found in this growth mode. Interestingly, in planktonic mode, the models suggest a consistent flow of galactose from the lactobacillus to the yeast, and of sucrose in minor amounts, with an amino acid flow from the yeast to the lactobacillus, as found by Ponomarova et al. (2017). Such a cross-feeding is more evident in M9, while in TSB the yeast gives away fewer amino acids, suggesting that this mutualistic interaction is stronger with fewer resources available in the environment, as would be expected (Supplementary Table 2). In biofilm mode, galactose exchange is pronounced, in both simple and complex media, consistent with its role in the extracellular matrix composition. The interaction between *L. reuteri* and *S. boulardii* would therefore seem more complex and dynamic than anticipated by the growth trends: the yeast might steal resources from the lactobacillus by growing faster, but at the same time the latter provides additional sugars to receive amino acid in return (also to grow the biofilm).

#### 4. Discussion

Both *L. reuteri* and *S. boulardii* are known to produce a wide variety of beneficial products for the host (Mu et al., 2018; Kelesidis and Potoulakis, 2012). In particular, *L. reuteri* produces reuterin and organic acids that have antimicrobial effects, while both species produce SCFAs and other immunomodulators that can suppress inflammation. Reuterin is a broad-spectrum antimicrobial compound that inhibits the growth of several harmful Gram-negative and Gram-positive bacteria, along with yeasts, moulds, and protozoa (Mu et al., 2018). Moreover, formate is an SCFA that has been found to help against cancer, immune system disorders, neurodegeneration and obesity (Pietzke et al., 2020), while L-lactate is involved in brain signalling (Mosienko et al., 2015) and isobutyrate in ulcerative colitis (Kedia et al., 2016). In addition, the biosynthesis of vitamins, amino acids, and enzymes can directly or indirectly benefit the host. For instance, some amino acids mentioned above are important for protein synthesis and a variety of other cellular functions (Neis et al., 2015). The three vitamins that belong to the vitamin B complex (B2, B3, B5), are essential for the proper development of the skin, lining of the digestive tract, blood cells, as well as our metabolism and brain function (Lukaski, 2004). Increased and stable production of such metabolites in the gut over a long period of time is expected to improve various aspects of human health, leading to probiotic supplements of high health value. As an example, probiotic administration was the primary factor influencing the gut microbiome of preterm infants in a large-scale longitudinal study (Beck et al., 2022). However, whether and how significant benefits can be provided in fully

developed intestinal microbiota is still to be understood. Firstly, even if beneficial metabolites are released in the gut, they could be re-absorbed by microbial partners eliminating the benefits for the host. Secondly, population levels of different species can change due to factors such as diet, host genetics, and environmental stimuli (e.g. exposure to antibiotics, acidity/alkalinity, etc.). From a clinical, translational perspective, the ability to improve the resilience of the gut microbial ecosystem prior to perturbations, or to restore its equilibrium afterwards, would offer significant benefits. To be effective, this therapeutic approach will likely need a personalised or subgroup-based understanding of individual genetics, diet, gut microbiome and other environmental factors that might be involved (Fassarella et al., 2021).

Several other studies have recently attempted to perform metabolic pathway reconstruction and gene expression or proteomic analysis in, for instance, *L. reuteri*, linking their results with its beneficial properties (Kristjansdottir et al., 2019; Saulnier et al., 2011; Mangiapane et al., 2014). Further, pairwise interactions among sets of bacteria have been reconstructed through co-culture growth experiments and metabolic modelling (Medlock et al., 2018). Here, the authors found that metabolite production and consumption generally decreased relative to the growth rate of each strain in pairs displaying positive interactions, suggesting that co-cultures with positive interactions can utilise resources more efficiently than co-cultures without positive interactions or mono-cultures. However, to our knowledge, our study is the first one taking into account the effects of growth mode (biofilm vs planktonic growth) on ecological interactions (mono-vs mixed cultures) in such an integrative experimental and modelling framework.

In the gut, nutrient availability, growth dynamics, oxygen gradients, and microbial community composition are different and much more complex (Donaldson et al., 2016). It is therefore important to highlight that our *in vitro* measurements only show specific metabolic effects under the tested conditions and *in vivo* studies are needed in order to confirm how the considered species behave. However, to our knowledge, only a few published *in vivo* studies focus on the metabolism of probiotic microbes (Liu et al., 2018). As biofilms are the main mode of coexistence in the gut, accounting for its metabolic demands can in principle better delineate the type of interactions that arise *in vivo* (Flemming et al., 2016). More generally, adopting an integrative approach along multiple biological factors can shed light on the complex and plastic nature of microbial interactions. While observed metabolic interactions are not guaranteed to take place *in vivo*, simplified and tractable probiotic ecosystems such as the one developed in this study can render them more accessible to experimental observations and mechanism identification. Our approach thus complements biomedical studies using direct probiotic administration Corbitt et al. (2018). Furthermore, with the computational method presented in this study, probiotic co-cultures could be optimised in such a way that they lead to increased levels of beneficial metabolites, prolonged production periods or even induction of synthesis of metabolites that are not normally produced in mono-cultures. This could enhance the biological and commercial values of certain probiotic products with a direct benefit for the probiotics industry Jangra et al. (2016). Finally, the effect of dietary interventions on the human gut microbiome can be better predicted and optimised with our method, potentially leading to the development of better treatment strategies for diseases associated with the gut microbiome, such as inflammatory bowel disease, obesity, type 2 diabetes, cardiovascular disease, autoimmune and neurological disorders Liu et al. (2018).

#### 5. Conclusions

In this study, we introduced an integrative approach for the genome-scale characterisation of microbial interactions in varying conditions, which was applied to investigate the metabolic ecology of *L. reuteri* and *S. boulardii* consortia. It was found that the production of specific microbial metabolites can be significantly affected by the growth mode, the

composition of the growth media, the microbial species and their interactions within a co-culture.

Moreover, the computational approach that was used here can lead to the design of new probiotic products and provide scientific insight for the application of metabolic engineering methods in order to optimise the production of desired beneficial metabolites. Such probiotic-based products are expected to be more effective, providing long-lasting health benefits and being used for the treatment or prevention of serious diseases such as inflammatory bowel disease, mental illnesses, obesity, diabetes, and cancer.

### CRedit authorship contribution statement

**Guido Zampieri:** Conceptualization, Methodology, Software, Validation, Formal analysis, Investigation, Data Curation, Writing - Original Draft, Writing - Review & Editing, Visualisation. **Georgios Efthimiou:** Conceptualization, Formal analysis, Investigation, Writing - Original Draft, Writing - Review & Editing, Resources, Funding acquisition. **Claudio Angione:** Conceptualization, Methodology, Writing - Review & Editing, Supervision, Project administration, Resources, Funding acquisition.

### Declaration of competing interest

The authors declare that they have no known competing financial interests or personal relationships that could have appeared to influence the work reported in this paper.

### Data availability

All the data and code has been shared as Supplementary Material

### Acknowledgements

This work was funded by UKRI Research England's THYME project. CA would also like to acknowledge a Network Development Award from The Alan Turing Institute, grant number TNDC2-100022.

### Appendix A. Supplementary data

Supplementary data to this article can be found online at <https://doi.org/10.1016/j.ymben.2023.01.008>.

### References

- Alshaiikh, B., Samara, J., Moossavi, S., Ferdous, T., Soraisham, A., Dersch-Mills, D., Arrieta, M.C., Amin, H., 2022. Multi-strain probiotics for extremely preterm infants: a randomized controlled trial. *Pediatr. Res.* 1–8.
- Antonakoudis, A., Strain, B., Barbosa, R., del Val, L.J., Kontoravdi, C., 2021. Synergising stoichiometric modelling with artificial neural networks to predict antibody glycosylation patterns in Chinese hamster ovary cells. *Comput. Chem. Eng.* 154, 107471.
- Arslan-Tontul, S., Erbas, M., 2020. Co-culture probiotic fermentation of protein-enriched cereal medium (boza). *J. Am. Coll. Nutr.* 39, 72–81.
- Basile, A., Campanaro, S., Kovalovszki, A., Zampieri, G., Rossi, A., Angelidaki, I., Valle, G., Treu, L., 2020. Revealing metabolic mechanisms of interaction in the anaerobic digestion microbiome by flux balance analysis. *Metab. Eng.* 62, 138–149.
- Bauer, E., Zimmermann, J., Baldini, F., Thiele, I., Kaleta, C., 2017. Bacarena: individual-based metabolic modelling of heterogeneous microbes in complex communities. *PLoS Comput. Biol.* 13, e1005544.
- Beaton, D., Dunlop, J., Abdi, H., 2016. Partial least squares correspondence analysis: a framework to simultaneously analyze behavioral and genetic data. *Psychol. Methods* 21, 621.
- Beaton, D., Fatt, C.R.C., Abdi, H., 2014. An exposition of multivariate analysis with the singular value decomposition in *r*. *Comput. Stat. Data Anal.* 72, 176–189.
- Beauvais, A., Loussert, C., Prevost, M.C., Verstrepen, K., Latgé, J.P., 2009. Characterization of a biofilm-like extracellular matrix in *fla1*-expressing *saccharomyces cerevisiae* cells. *FEMS Yeast Res.* 9, 411–419.
- Beck, L.C., Masi, A.C., Young, G.R., Vatanen, T., Lamb, C.A., Smith, R., Coxhead, J., Butler, A., Marsland, B.J., Embleton, N.D., et al., 2022. Strain-specific impacts of probiotics are a significant driver of gut microbiome development in very preterm infants. *Nat. Microbiol.* 7, 1525–1535.
- Benjamini, Y., Hochberg, Y., 1995. Controlling the false discovery rate: a practical and powerful approach to multiple testing. *J. Roy. Stat. Soc. B* 57, 289–300.
- Botev, Z.I., 2017. The normal law under linear restrictions: simulation and estimation via minimax tilting. *J. Roy. Stat. Soc. B* 79, 125–148.
- Braunstein, A., Muntoni, A.P., Pagnani, A., 2017. An analytic approximation of the feasible space of metabolic networks. *Nat. Commun.* 8, 1–9.
- Chapman, C., Gibson, G.R., Rowland, I., 2012. In vitro evaluation of single- and multi-strain probiotics: Inter-species inhibition between probiotic strains, and inhibition of pathogens. *Anaerobe* 18, 405–413.
- Colarusso, A.V., Goodchild-Michelman, I., Rayle, M., Zomorrodi, A.R., 2021. Computational modeling of metabolism in microbial communities on a genome-scale. *Curr. Opin. Struct. Biol.* 26, 46–57.
- Corbitt, M., Campagnolo, N., Staines, D., Marshall-Gradsnik, S., 2018. A systematic review of probiotic interventions for gastrointestinal symptoms and irritable bowel syndrome in chronic fatigue syndrome/myalgic encephalomyelitis (cfs/me). *Probiotics Antimicrob. Proteins* 10, 466–477.
- Coyte, K.Z., Rakoff-Nahoum, S., 2019. Understanding competition and cooperation within the mammalian gut microbiome. *Curr. Biol.* 29, R538–R544.
- Culley, C., Vijayakumar, S., Zampieri, G., Angione, C., 2020. A mechanism-aware and multiomic machine-learning pipeline characterizes yeast cell growth. *Proc. Natl. Acad. Sci. USA* 117, 18869–18879.
- Dalile, B., Van Oudenhove, L., Vervliet, B., Verbeke, K., 2019. The role of short-chain fatty acids in microbiota–gut–brain communication. *Nat. Rev. Gastroenterol. Hepatol.* 16, 461–478.
- De Vrese, M., Schrezenmeir, J., 2008. Probiotics, prebiotics, and synbiotics. *Food Biotechnol.* 1–66.
- Donaldson, G.P., Lee, S.M., Mazmanian, S.K., 2016. Gut biogeography of the bacterial microbiota. *Nat. Rev. Microbiol.* 14, 20–32.
- Dysvik, A., La Rosa, S.L., Liland, K.H., Myhrer, K.S., Østlie, H.M., De Rouck, G., Rukke, E. O., Westereng, B., Wicklund, T., 2020. Co-fermentation involving *saccharomyces cerevisiae* and *lactobacillus* species tolerant to brewing-related stress factors for controlled and rapid production of sour beer. *Front. Microbiol.* 11, 279.
- Fang, X., Lloyd, C.J., Palsson, B.O., 2020. Reconstructing organisms in silico: genome-scale models and their emerging applications. *Nat. Rev. Microbiol.* 18, 731–743.
- Faria-Oliveira, F., Carvalho, J., Belmiro, C.L., Ramalho, G., Pavão, M., Lucas, C., Ferreira, C., 2015. Elemental biochemical analysis of the polysaccharides in the extracellular matrix of the yeast *saccharomyces cerevisiae*. *J. Basic Microbiol.* 55, 685–694.
- Fassarella, M., Blaak, E.E., Penders, J., Nauta, A., Smidt, H., Zoetendal, E.G., 2021. Gut microbiome stability and resilience: elucidating the response to perturbations in order to modulate gut health. *Gut* 70, 595–605.
- Fleming, H.C., Wingender, J., Szewzyk, U., Steinberg, P., Rice, S.A., Kjelleberg, S., 2016. Biofilms: an emergent form of bacterial life. *Nat. Rev. Microbiol.* 14, 563.
- Foligné, B., Parayre, S., Cheddani, R., Famelart, M.H., Madec, M.N., Plé, C., Breton, J., Dewulf, J., Jan, G., Deutsch, S.M., 2016. Immunomodulation properties of multi-species fermented milks. *Food Microbiol.* 53, 60–69.
- Frese, S.A., MacKenzie, D.A., Peterson, D.A., Schmaltz, R., Fangman, T., Zhou, Y., Zhang, C., Benson, A.K., Cody, L.A., Mulholland, F., et al., 2013. Molecular characterization of host-specific biofilm formation in a vertebrate gut symbiont. *PLoS Genet.* 9, e1004057.
- Ghosh, S., Chowdhury, R., Bhattacharya, P., 2016. Mixed consortia in bioprocesses: role of microbial interactions. *Appl. Microbiol. Biotechnol.* 100, 4283–4295.
- Han, S., Lu, Y., Xie, J., Fei, Y., Zheng, G., Wang, Z., Liu, J., Lv, L., Ling, Z., Berglund, B., et al., 2021. Probiotic gastrointestinal transit and colonization after oral administration: a long journey. *Front. Cell. Infect. Microbiol.* 11, 102.
- Heirendt, L., Arreckx, S., Pfau, T., Mendoza, S.N., Richelle, A., Heinken, A., Haraldsdóttir, H.S., Wachowiak, J., Keating, S.M., Vlasov, V., et al., 2019. Creation and analysis of biochemical constraint-based models using the cobra toolbox v. 3.0. *Nat. Protoc.* 14, 639–702.
- Jangra, M., Belur, P.D., Oriabinska, L.B., Dugan, O.M., 2016. Multistrain probiotic production by co-culture fermentation in a lab-scale bioreactor. *Eng. Life Sci.* 16, 247–253.
- Jarosz, D.F., Brown, J.C., Walker, G.A., Datta, M.S., Ung, W.L., Lancaster, A.K., Rotem, A., Chang, A., Newby, G.A., Weitz, D.A., et al., 2014. Cross-kingdom chemical communication drives a heritable, mutually beneficial prion-based transformation of metabolism. *Cell* 158, 1083–1093.
- Jin, X., Chen, W., Chen, H., Chen, W., Zhong, Q., 2019. Combination of *lactobacillus plantarum* and *saccharomyces cerevisiae* dv10 as starter culture to produce mango slurry: microbiological, chemical parameters and antioxidant activity. *Molecules* 24, 4349.
- Jo, J., Price-Whelan, A., Dietrich, L.E., 2022. Gradients and consequences of heterogeneity in biofilms. *Nat. Rev. Microbiol.* 1–15.
- Kaleta, C., Schäuble, S., Rinas, U., Schuster, S., 2013. Metabolic costs of amino acid and protein production in *escherichia coli*. *Biotechnol. J.* 8, 1105–1114.
- Kedia, S., Rampal, R., Paul, J., Ahuja, V., 2016. Gut microbiome diversity in acute infective and chronic inflammatory gastrointestinal diseases in north India. *J. Gastroenterol.* 51, 660–671.
- Kelesidis, T., Pothoulakis, C., 2012. Efficacy and safety of the probiotic *saccharomyces boulardii* for the prevention and therapy of gastrointestinal disorders. *Therapeut. Adv. Gastroenterol.* 5, 111–125.
- Khatiri, I., Tomar, R., Ganesan, K., Prasad, G., Subramanian, S., 2017. Complete genome sequence and comparative genomics of the probiotic yeast *saccharomyces boulardii*. *Sci. Rep.* 7, 1–12.
- King, Z.A., Lu, J., Dräger, A., Miller, P., Federowicz, S., Lerman, J.A., Ebrahim, A., Palsson, B.O., Lewis, N.E., 2016. Bigg models: a platform for integrating, standardizing and sharing genome-scale models. *Nucleic Acids Res.* 44, D515–D522.

- Kristjansdóttir, T., Bosma, E.F., Dos Santos, F.B., Özdemir, E., Herrgård, M.J., França, L., Ferreira, B., Nielsen, A.T., Gudmundsson, S., 2019. A metabolic reconstruction of *Lactobacillus reuteri* jcm 1112 and analysis of its potential as a cell factory. *Microb. Cell Factories* 18, 1–19.
- Kumar, H., Salminen, S., Verhagen, H., Rowland, I., Heimbach, J., Bañares, S., Young, T., Nomoto, K., Lalonde, M., 2015. Novel probiotics and prebiotics: road to the market. *Curr. Opin. Biotechnol.* 32, 99–103.
- Lee, K., Lee, H.G., Pi, K., Choi, Y.J., 2008. The effect of low pH on protein expression by the probiotic bacterium *Lactobacillus reuteri*. *Proteomics* 8, 1624–1630.
- Liu, J., Shi, P., Ahmad, S., Yin, C., Liu, X., Liu, Y., Zhang, H., Xu, Q., Yan, H., Li, Q., 2019. Co-culture of *Bacillus coagulans* and *Candida utilis* efficiently treats *Lactobacillus* fermentation wastewater. *Amb. Express* 9, 1–6.
- Liu, Y., Tran, D.Q., Rhoads, J.M., 2018. Probiotics in disease prevention and treatment. *J. Clin. Pharmacol.* 58, S164–S179.
- Lukaski, H.C., 2004. Vitamin and mineral status: effects on physical performance. *Nutrition* 20, 632–644.
- Machado, D., Andrejev, S., Tramontano, M., Patil, K.R., 2018. Fast automated reconstruction of genome-scale metabolic models for microbial species and communities. *Nucleic Acids Res.* 46, 7542–7553.
- Machado, D., Maistrenko, O.M., Andrejev, S., Kim, Y., Bork, P., Patil, K.R., Patil, K.R., 2021. Polarization of microbial communities between competitive and cooperative metabolism. *Nat. Ecol. Evol.* 5, 195–203.
- Magnúsdóttir, S., Heinken, A., Kutt, L., Ravcheev, D.A., Bauer, E., Noronha, A., Greenhalgh, K., Jäger, C., Baginska, J., Wilmes, P., et al., 2017. Generation of genome-scale metabolic reconstructions for 773 members of the human gut microbiota. *Nat. Biotechnol.* 35, 81–89.
- Mangiapan, E., Lamberti, C., Pessione, A., Galano, E., Amoresano, A., Pessione, E., 2014. Selenium effects on the metabolism of a se-metabolizing *Lactobacillus reuteri*: analysis of envelope-enriched and extracellular proteomes. *Mol. Biosyst.* 10, 1272–1280.
- Medlock, G.L., Carey, M.A., McDuffie, D.G., Mundy, M.B., Giallourou, N., Swann, J.R., Kolling, G.L., Papin, J.A., 2018. Inferring metabolic mechanisms of interaction within a defined gut microbiota. *Cell Syst.* 7, 245–257.
- Mendoza, S.N., Olivier, B.G., Molenaar, D., Teusink, B., 2019. A systematic assessment of current genome-scale metabolic reconstruction tools. *Genome Biol.* 20, 1–20.
- Mills, E., O'Neill, L.A., 2014. Succinate: a metabolic signal in inflammation. *Trends Cell Biol.* 24, 313–320.
- Mo, M.L., Palsson, B.Ø., Herrgård, M.J., 2009. Connecting extracellular metabolomic measurements to intracellular flux states in yeast. *BMC Syst. Biol.* 3, 1–17.
- Moretti, S., Tran, V.D.T., Mehl, F., Ibberson, M., Pagni, M., 2021. Metanetx/mnxref: unified namespace for metabolites and biochemical reactions in the context of metabolic models. *Nucleic Acids Res.* 49, D570–D574.
- Mosienko, V., Teschemacher, A.G., Kasparov, S., 2015. Is l-lactate a novel signaling molecule in the brain? *J. Cerebr. Blood Flow Metabol.* 35, 1069–1075.
- Mu, Q., Tavella, V.J., Luo, X.M., 2018. Role of *Lactobacillus reuteri* in human health and diseases. *Front. Microbiol.* 9, 757.
- Neis, E.P., Dejong, C.H., Rensen, S.S., 2015. The role of microbial amino acid metabolism in host metabolism. *Nutrients* 7, 2930–2946.
- Occhipinti, A., Eyassu, F., Rahman, T.J., Rahman, P.K., Angione, C., 2018. In silico engineering of *Pseudomonas* metabolism reveals new biomarkers for increased biosurfactant production. *PeerJ* 6, e6046.
- Pais, P., Almeida, V., Yilmaz, M., Teixeira, M.C., 2020. *Saccharomyces boulardii*: what makes it tick as successful probiotic? *J. Fungi* 6, 78.
- Peres-Neto, P.R., Jackson, D.A., Somers, K.M., 2005. How many principal components? stopping rules for determining the number of non-trivial axes revisited. *Comput. Stat. Data Anal.* 49, 974–997.
- Pietzke, M., Meiser, J., Vazquez, A., 2020. Formate metabolism in health and disease. *Mol. Metabol.* 33, 23–37.
- Pio, G., Mignone, P., Magazzù, G., Zampieri, G., Ceci, M., Angione, C., 2022. Integrating genome-scale metabolic modelling and transfer learning for human gene regulatory network reconstruction. *Bioinformatics* 38, 487–493.
- Ponomarova, O., Gabrielli, N., Sévin, D.C., Müller, M., Zirngibl, K., Bulyha, K., Andrejev, S., Kafkia, E., Typas, A., Sauer, U., et al., 2017. Yeast creates a niche for symbiotic lactic acid bacteria through nitrogen overflow. *Cell Syst.* 5, 345–357.
- Ribaudo, N., Li, X., Davis, B., Wood, T.K., Huang, Z., 2017. A genome-scale modeling approach to quantify biofilm component growth of *Salmonella typhimurium*. *J. Food Sci.* 82, 154–166.
- Rima, H., Steve, L., Ismail, F., 2012. Antimicrobial and probiotic properties of yeasts: from fundamental to novel applications. *Front. Microbiol.* 3, 421.
- Salas-Jara, M.J., Ilabaca, A., Vega, M., García, A., 2016. Biofilm forming *Lactobacillus*: new challenges for the development of probiotics. *Microorganisms* 4, 35.
- Saulnier, D.M., Santos, F., Roos, S., Mistretta, T.A., Spinler, J.K., Molenaar, D., Teusink, B., Versalovic, J., 2011. Exploring metabolic pathway reconstruction and genome-wide expression profiling in *Lactobacillus reuteri* to define functional probiotic features. *PLoS One* 6, e18783.
- Seaver, S.M., Liu, F., Zhang, Q., Jeffries, J., Faria, J.P., Edirisinghe, J.N., Mundy, M., Chia, N., Noor, E., Beber, M.E., et al., 2021. The modelseed biochemistry database for the integration of metabolic annotations and the reconstruction, comparison and analysis of metabolic models for plants, fungi and microbes. *Nucleic Acids Res.* 49, D575–D588.
- Terraf, M.C.L., Tomás, M.S.J., Rault, L., Le Loir, Y., Even, S., Nader-Macías, M.E.F., 2016. Biofilms of vaginal *Lactobacillus reuteri* crl 1324 and *Lactobacillus rhamnosus* crl 1332: kinetics of formation and matrix characterization. *Arch. Microbiol.* 198, 689–700.
- Thiele, I., Sahoo, S., Heinken, A., Hertel, J., Heirendt, L., Aurich, M.K., Fleming, R.M., 2020. Personalized whole-body models integrate metabolism, physiology, and the gut microbiome. *Mol. Syst. Biol.* 16, e8982.
- Toscano, M., De Grandi, R., Pastorelli, L., Vecchi, M., Drago, L., 2017. A consumer's guide for probiotics: 10 golden rules for a correct use. *Dig. Liver Dis.* 49, 1177–1184.
- Vázquez-Castellanos, J.F., Biclôt, A., Vrancken, G., Huys, G.R., Raes, J., 2019. Design of synthetic microbial consortia for gut microbiota modulation. *Curr. Opin. Pharmacol.* 49, 52–59.
- Vijayakumar, S., Conway, M., Lió, P., Angione, C., 2018. Optimization of multi-omic genome-scale models: Methodologies, hands-on tutorial, and perspectives. *Metabol. Netw. Reconstruct. Model.* 389–408.
- Vijayakumar, S., Rahman, P.K., Angione, C., 2020. A hybrid flux balance analysis and machine learning pipeline elucidates metabolic adaptation in cyanobacteria. *iScience* 23, 101818.
- Vital-Lopez, F.G., Reifman, J., Wallqvist, A., 2015. Biofilm formation mechanisms of *Pseudomonas aeruginosa* predicted via genome-scale kinetic models of bacterial metabolism. *PLoS Comput. Biol.* 11, e1004452.
- Woodward, M.J., Sojka, M., Spriggins, K.A., Humphrey, T.J., 2000. The role of sef14 and sef17 fimbriae in the adherence of *Salmonella enterica* serotype enteritidis to inanimate surfaces. *J. Med. Microbiol.* 49, 481–487.
- Zampieri, G., Vijayakumar, S., Yaneske, E., Angione, C., 2019. Machine and deep learning meet genome-scale metabolic modeling. *PLoS Comput. Biol.* 15, e1007084.
- Zhang, J., Petersen, S.D., Radivojevic, T., Ramirez, A., Pérez-Manríquez, A., Abeliuk, E., Sánchez, B.J., Costello, Z., Chen, Y., Fero, M.J., et al., 2020. Combining mechanistic and machine learning models for predictive engineering and optimization of tryptophan metabolism. *Nat. Commun.* 11, 1–13.
- Zomorodi, A.R., Islam, M.M., Maranas, C.D., 2014. d-optcom: dynamic multi-level and multi-objective metabolic modeling of microbial communities. *ACS Synth. Biol.* 3, 247–257.